

Redox-responsive chemosensitive polyspermine delivers ursolic acid targeting to human breast tumor cells: The depletion of intracellular GSH contents arouses chemosensitizing effects



Xin Ji^a, Qiao Tang^a, Peng Pang^d, Jianping Wu^b, Thomas Brett Kirk^b, Jiake Xu^c, Dong Ma^{a,*}, Wei Xue^{a,*}

^a Key Laboratory of Biomaterials of Guangdong Higher Education Institutes, Department of Biomedical Engineering, Jinan University, Guangzhou 510632, China

^b 3D Imaging and Bioengineering Laboratory, Department of Mechanical Engineering, Curtin University, Australia

^c The School of Pathology and Laboratory Medicine, University of Western Australia, Perth, Australia

^d College of Traditional Chinese Medicine, Jinan University, Guangzhou 510632, China

ARTICLE INFO

Keywords:

Polymeric prodrug
Chemosensitivity
Ursolic acid
Targeted delivery
Cancer therapy

ABSTRACT

Antitumor efficacy of ursolic acid (UA) is seriously limited due to its low hydrophilicity and needy bioavailability. To overcome these obstacles, chemosensitive polyspermine (CPSP) conjugated with UA and folic acid (FA) as a novel targeted prodrug was designed and successfully synthesized in this investigation. This prodrug not only showed high aqueous solubility, GSH-triggered degradation and good biocompatibility, but also exhibited better inhibition effect on the tumor cells proliferation in comparison with free UA. FA-CPSP-UA could down-regulate the generation of GSH and manifest excellent ability in enhancing antitumor efficacy. In addition, FA-CPSP-UA could inhibit the expression of MMP-9, which led to restricting MCF-7 cells migration. Taken together, the results indicated that FA-CPSP-UA, as a carrier, can efficiently deliver UA to folate receptor positive cancer cells and improve tumor therapy of UA by Chemosensitive effect.

1. Introduction

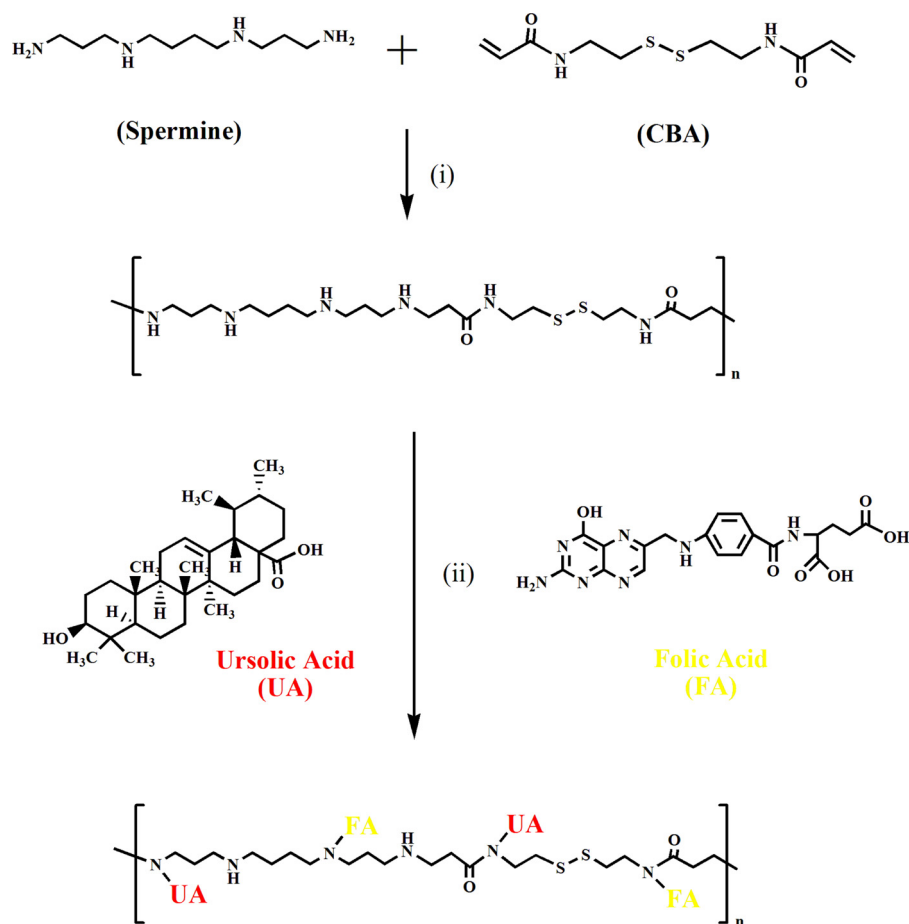
Ursolic acid (UA), as a pentacyclic triterpenic acid, widespread in a large number of natural medicinal plants with multiple pharmacological properties, including anti-inflammatory, liver-protective, anti-atherosclerotic, anti-epileptic, anti-cancer, anti-epileptic, and anti-diabetic activities [1–6]. Various papers have shown that UA exhibits excellent anti-tumor effect, mainly through the induction of apoptosis, inhibition of tumor cell proliferation, suppression of tumor tissue angiogenesis, repression of tumor invasion and metastasis, interference with tumor micro-environment and other effects to achieve the purpose of anti-tumor [7–10]. Pharmacology research shows that UA can inhibit the proliferation and induce apoptosis in MCF-7 human breast cancer cells [7,11]. However, the potential clinical applications of UA are ultimately obstructed due to its low hydrophilicity, non-specific distribution and poor bioavailability. To address these limitations, the great efforts had been devoted to improving anticancer efficacy of UA by designing intelligent drug delivery systems. Recently, various drug delivery systems such as polymeric nanoparticles, phospholipid nanoparticles, micellar nanosystems and liposomes have attracted increasing

attention since their remarkable superiority in enhancing antitumor efficacy in cancer treatment [12–16].

To devise the excellent drug delivery systems, quite a few strategies are proposed: (i) targeting molecules have been introduced to stimulate cellular uptake by targeting nanocarriers to specific receptors out of the cell surface; (ii) combining a sensitizer (drug) with prodrugs to increase chemosensitivity to UA [17–20]. The folate receptors are overexpressed in many cancer cells, including breast, ovary, endometrium, kidney, lung, head and neck, myeloid cancers and so on [21,22]. Meanwhile, they are internalized into cells after ligand binding [23]. Because of absence or low expression of these receptors on normal tissues, folate-linked carrier system does not normally accumulate in healthy tissues. Compared with over other ligands, the advantages of FA are high affinity and specificity towards receptors, good conjugating property, low cost, easy availability and non-immunogenicity [24]. Moreover, glutathione (GSH) acts as antioxidant and protects cells against reactive oxygen species (ROS) and xenobiotics (heavy metals and drug metabolites, etc.) [25,26]. GSH-mediated detoxification is one of the most major mechanisms responsible for the cancer drug resistance and the GSH levels in tumor cells are comparatively higher than those in normal

* Corresponding authors.

E-mail addresses: tmadong@jnu.edu.cn, madong_jnu@163.com (D. Ma), weixue_jnu@aliyun.com (W. Xue).



Scheme 1. Synthesis scheme of the FA-CPSP-UA conjugate using folic acid (FA), ursolic acid (UA), and chemosensitive polyspermine (CPSP).

cells [27]. It has been observed that elevated levels of GSH are associated with resistance to chemotherapeutic agents in cancer cells [28]. As a drug sensitizer in combination therapy with chemotherapeutic agent, buthionine sulfoximine (BSO) can selectively inhibit the synthesis of GSH to reduce the GSH-mediated detoxification [29]. In addition, utilizing the concentration difference of the GSH in the bloodstream ($< 5 \mu\text{M}$) and the cytosol of cancer cells (up to 2–10 mM), the redox-cleavable disulfide bonds were introduced to improve intracellular drug release in response to intracellular levels of GSH [30–33].

In order to effectively treat human breast cancer by combining the sensitizer with prodrug, we designed and synthesized the GSH-triggered degradable FA-targeted chemosensitive polyspermine prodrug (FA-CPSP-UA) for UA delivery in which UA was loaded by chemical conjugation (Scheme 1). The strong hydrophilic properties of CPSP made UA well dispersed in water [34]. The conjugation FA of prodrug could provide active targeting and enhance cellular uptake of the prodrug, which greatly increased tumor specificity and highly improved drug efficacy. The high intracellular GSH concentration facilitated FA-CPSP-UA degradation by segmentation of a large of disulfide bonds, which extremely enhanced intracellular drug release. Moreover, the large intracellular GSH was consumed in the course of the degradation process, which reduced the GSH-mediated detoxification and promoted the chemotherapeutic efficacy. Compared to free UA, the FA-CPSP-UA not only showed better inhibition effect on the MCF-7 cells proliferation, but exhibited excellent ability in inhibiting the migration of MCF-7 cells. Therefore, because of its self-sensibilization effect and prominent anticancer activity, the FA-CPSP-UA provides a promising strategy for treating breast cancer.

2. Materials and methods

2.1. Materials

Spermine, acryloyl chloride, cystamine dihydrochloride, *N,N'*-bis(acryloyl) cystamine (BAC), *N*-hydroxysuccinimide (NHS), *N*-(3-Dimethylaminopropyl)-*N'*-ethylcarbodiimide hydrochloride (EDC-HCl), folic acid (FA), *L*-buthionine-S,*R*-sulfoximine (BSO), and ursolic acid (UA) were purchased from Aladdin-reagent Company (Shanghai, China) and used directly. Methanol, dichloromethane and sodium hydroxide were purchased from Guangzhou Chemical Reagent (China). Dulbecco's modified Eagle's medium (DMEM) and Dulbecco's phosphate buffered saline (PBS) were purchased from Life Technologies Corporation. Reduced glutathione assay kit was purchased from Nanjing Jiancheng Bioengineer Institute. Cell counting kit-8 (CCK-8) and Annexin V-FITC Apoptosis Detection Kit were purchased from Beyotime Institute of Biotechnology (Shanghai, China).

2.2. Cell culture

The MCF-7 human breast cancer cells were obtained from Southern Medical University. MCF-7 cells were cultured in complete DMEM (with 10% FBS, 100 U/mL penicillin G sodium and 0.1 mg/mL streptomycin sulfate). Cells were maintained at 37 °C in a humid atmosphere containing 5% CO₂.

2.3. Synthesis of CPSP

The synthetic route of FA-CPSP-UA is showed in Scheme 1. For CPSP synthesis, we first synthesized, *N,N'*-bis(acryloyl) cystamine (BAC) in

accordance with our previous study [35]. In brief, cystamine dihydrochloride (2.5 g, 11.10 mmol) was dissolved in 11 mL distilled water. Then, 6.6 mL acryloyl chloride solution in dichloromethane (v/v = 1/1) and 4.4 mL aqueous NaOH solution (0.40 g/mL) were added dropwise with stirring in the ice bath. Subsequently, the mixture was stirred at room temperature for another 6 h. The mixture was extracted with dichloromethane and washed by distilled water. Subsequently, CBA was obtained with a yield of 75% after the organic solvent was removed under reduced pressure. ^1H NMR (CDCl_3): $\delta = 6.25$ ppm (4H, $\text{CH}_2=\text{CHCO}-$), $\delta = 5.68$ ppm (2H, $\text{CH}_2=\text{CHCO}$), $\delta = 3.67$ ppm (4H, $\text{CO}-\text{NH}-\text{CH}_2-\text{CH}_2-\text{S}-$), $\delta = 2.90$ ppm (4H, $\text{CO}-\text{NH}-\text{CH}_2-\text{CH}_2-\text{S}-$).

CPSP was synthesized by Michael addition polymerization of CBA and spermine. CBA (0.524 g, 2 mmol) and Spermine (0.608 g, 3 mmol) was separately dissolved in freshly prepared 5 mL methanol/water (v/v = 3/1) solution containing 100 mM calcium chloride at room temperature. After that, the spermine solution was then added dropwise to the CBA solution with stirring under a nitrogen atmosphere. The mixture reacted at 50 °C for 72 h in dark. After completion of reaction, the solvent was removed by rotary evaporation and the residue was dialyzed (MWCO = 3500, USA) for 3 d in dark. The synthesized CPSP was obtained by lyophilization with a yield of 62%. ^1H NMR (D_2O): $\delta = 1.6$ ppm ($-\text{CH}_2-$), $\delta = 1.98$ ppm ($-\text{CH}_2-\text{CH}_2-$), $\delta = 2.99$ ppm ($-\text{S}-\text{CH}_2-$), $\delta = 3.44$ ppm ($\text{CO}-\text{NH}-\text{CH}_2-$), $\delta = 2.77$ ppm ($-\text{NH}-\text{CH}_2-$), $\delta = 3.44$ ppm ($-\text{CO}-\text{NH}-\text{CH}_2-$).

2.4. Synthesis of CPSP-conjugating FA and UA (FA-CPSP-UA)

FA-CPSP-UA has been synthesized by coupling UA and FA onto CPSP via EDC-HCl / NHS. Briefly, both FA (4 mg, 0.0091 mmol) and UA (6 mg, 0.013 mmol) were dissolved in DMSO (0.5 mL), and then were activated by EDC-HCl (17.64 mg, 0.092 mmol) and NHS (10.59 mg, 0.092 mmol). After its pH value was adjusted to 4 ~ 6 by HCl, the mixture was stirred at 25 °C for 1 h. After that CPSP (100 mg) was added to the reaction mixture of activated FA and UA [36]. The reaction continued at 25 °C for 24 h in the dark conditions. Finally, to remove free FA and UA, the resultant solution was kept in a pretreated dialysis bag (MWCO = 1000, USA) and dialyzed for 12 h. FA-CPSP-UA was obtained by freeze drying with a yield of 49%.

2.5. Structural characterizations of FA-CPSP-UA

^1H NMR spectra of CBA, CPSP and FA-CPSP-UA were obtained from a Bruker AVANCE 300 spectrometer (300 MHz). UV-vis spectrum (UV-2550, Shimadzu, Japan) was employed to confirm the graft of UA and FA to CPSP and the mass content. FA, UA, CPSP and FA-CPSP-UA were dissolved in sodium hydroxide solution (0.1 mol/L). Then, UV-vis spectrum of FA, UA, CPSP and FA-CPSP-UA were recorded on a 1 cm quartz cuvette at 25 °C. What's more, the mean particle size and zeta potential of CPSP, UA-CPSP and FA-CPSP-UA at 100 $\mu\text{g}/\text{mL}$ were determined by Malvern Zetasizer Nano ZS (United Kingdom). Each sample was measured in triplicate. Subsequently, the morphology was characterized by a transmission electron microscope (TEM). For GSH-response analysis, the elution time of FA-CPSP-UA pretreated either with or without 10 mM GSH were determined by GPC.

2.6. In vitro drug release behavior of FA-CPSP-UA

To determine the release of UA from FA-CPSP-UA *in vitro*, the dialysis method was applied to monitor the release of UA from FA-CPSP-UA in PBS (20% (v/v) ethanol, with or without 10 mM GSH) at pH 7.4 and 37 °C. The lyophilized FA-CPSP-UA (20 mg) was suspended in 2 mL of 0.1 M PBS containing 20% of ethanol. The half of solution was then placed into pre-swelled dialysis bag (MWCO = 1000, USA) and immersed into 30 mL of 0.1 M PBS (with or without 10 mM GSH) at the presence of ethanol. The release study of free UA was performed under the same condition with adding 1 mg UA suspended in 2 mL of 0.1 M

PBS containing 20% of ethanol in the dialysis bag. The quantity of UA released was analyzed by UV-vis spectrum (UV-2550, Shimadzu, Japan) at a wavelength of 265 nm at various time points during the dialysis process. After subtracting the absorbance of FA, the cumulative release of UA was calculated by comparing with the standard curve.

The cumulative release of UA was calculated using the formula:

$$\text{Release percentage (\%)} = \text{W1}/\text{W0} \times 100\%$$

where W1 was the weight of UA in solution, W0 was the weight of total UA in prodrugs.

2.7. FA-targeting assay

CPSP-UA and FA-CPSP-UA were marked with FITC by the method reported in the literature [37]. The obtained FI-CPSP-UA and FI-FA-CPSP-UA were incubated with MCF-7 cells for FA-targeting examination. To determine the role of FR binding, MCF-7 cells were pretreated without or with 250 μg and 500 μg of free FA in 500 μL culture medium. After 2 h, the culture medium was replaced for 500 μL complete DMEM that contained 5 μg of FA-CPSP-FITC and CPSP-FITC, respectively. MCF-7 cells were then incubated for 4 h and the cellular uptake percentages were calculated by flow cytometer (Backman).

2.8. Determination of the GSH level

Intracellular GSH concentration in MCF-7 cells were detected by using Reduced glutathione assay kit. The growth medium was replaced with 500 μL complete DMEM that contained free UA (10 μg), FA-CPSP-UA (64 μg), BSO (5×10^{-4} mmol), FA-CPSP (55 μg) and the mixture of BSO (5×10^{-4} mmol) and UA (10 μg), respectively. For ensuring the comparison of the experiment, the corresponding concentration of FA-CPSP-UA is calculated according to the grafting rate of UA. After co-incubation for 24 h, the medium was removed. After washing with PBS for three times, the cells were lysed. The intracellular GSH level was strictly examined using the abovementioned kit according to the manufacturer's instruction.

2.9. In vitro cytotoxicity assay

The cytotoxicity of free UA and FA-CPSP-UA was evaluated in MCF-7 cells using CCK-8 assay [38]. CPSP (1, 10, 100, 200, 400 $\mu\text{g}/\text{mL}$), FA-CPSP (1, 10, 100, 200, 400 $\mu\text{g}/\text{mL}$), free UA, UA-CPSP or FA-CPSP-UA was added to the cells in DMEM at different UA concentrations of 1, 10, 25, 50, and 100 $\mu\text{g}/\text{mL}$, respectively. Moreover, in order to assess the effect of intracellular GSH concentration on anti-cancer activity, BSO (1 mmol/L), GSH (10 mmol/L), GSH/UA (20 $\mu\text{g}/\text{mL}$), free UA (20 $\mu\text{g}/\text{mL}$), BSO/UA (20 $\mu\text{g}/\text{mL}$) or FA-CPSP-UA (99 $\mu\text{g}/\text{mL}$) was added to complete DMEM to final concentrations. Cells treated with PBS were used as a control. After MCF-7 cells were incubated for 24 h, cells were washed with PBS and added with 100 μL fresh medium containing 10% CCK-8 to all wells. The absorbance was recorded with a microplate reader at a wavelength of 450 nm and the cell viability was expressed as a ratio of the treated groups to the control group.

2.10. Cell apoptosis assay

The quantification of cell apoptosis was performed by Annexin V/PI staining and evaluated by flow cytometer [39]. Briefly, MCF-7 cells were seeded in 24-well tissue culture plates at a density of 5×10^4 cells/well and cultured in complete DMEM at 37 °C in 5% CO_2 for 12 h. The cells were incubated with various formulations (free UA: 20 $\mu\text{g}/\text{mL}$, CPSP: 100 $\mu\text{g}/\text{mL}$, UA-CPSP: 89 $\mu\text{g}/\text{mL}$, FA-CPSP-UA: 99 $\mu\text{g}/\text{mL}$) for 24 h, respectively. Then the cells were immediately trypsinized, collected and resuspended in 200 μL of binding buffer. Afterwards, 5 μL of Annexin V-FITC and 10 μL of PI were added and kept in the dark for

15 min. The stained cells were analyzed using flow cytometer (Backman).

2.11. Wound healing assay

To study the ability of FA-CPSP-UA to inhibit MCF-7 cells migration, a wound healing assay was conducted [40]. MCF-7 cells were seeded at a density of 2×10^5 cells/well with 2 mL complete DMEM onto 6-well tissue culture plates for 12 h. After starved with serum-free DMEM for about 6 h, the cells were wounded by pipette tips and washed with PBS twice times. Subsequently, the cells were incubated in fresh complete DMEM with various concentrations of FA-CPSP-UA for 24 h. Cells treated with PBS were used as control. The cell migration into the scratches was observed under microscope and analyzed with the software of ImageJ.

2.12. Western blot

The influence of FA-CPSP-UA on the expression levels of MMP-9 protein in MCF-7 cells was analyzed by western blotting [41]. MCF-7 cells were incubated for 24 h with various concentrations of FA-CPSP-UA for exploring the expression of MMP-9. After that, cells were washed twice with cold PBS and lysed with SDS lysis buffer for 30 min on ice. Then the lysates was clarified by centrifugation at 4 °C under 13,000 rpm/min for 15 min, and the supernatant was collected. Protein concentrations were determined using the Bio-Rad protein assay. Sodium dodecyl sulfate polyacrylamide gel electrophoresis was performed to separate the samples and then transferred to PVDF membranes (Bio-Rad). The membranes were blocked with 5% non-fat milk in Tris-Buffered Saline Tween-20 (TBST) buffer for 1 h. Then the membranes were incubated with MMP-9 antibodies at 1:1000 dilution in 5% non-fat milk overnight at 4 °C. Then the membranes were incubated with secondary antibodies at 1:2000 dilution for 1 h at 25 °C, followed by three times washing with TBST. Afterwards the sample was detected by using enhanced chemiluminescence reagent (Bio-Rad), and GAPDH was used as a control.

2.13. Hemolysis

For validating the blood compatibility of FA-CPSP-UA, an hemolysis assay was performed as previously reported [42]. The percentage hemolysis was calculated by measuring the optical density (OD) as the following formula:

$$\text{Hemolysis (\%)} = [(\text{OD of the test sample} - \text{OD of negative control}) \times 100] / \text{OD of positive control.}$$

2.14. Statistical analysis

All experiments were carried out at least in triplicate and the acquired data were presented as the mean \pm standard deviation (SD). Statistical analysis was performed using a Student's *t*-test (SPSS, version 22.0). Difference with $P < 0.05$ (*), $P < 0.01$ (**) or $P < 0.001$ (***) was considered statistically significant.

3. Results and discussion

3.1. Synthesis and characterization of FA-CPSP-UA

In the present study, CPSP was used as the starting material to synthesize the targeted anticancer prodrug FA-CPSP-UA and the synthetic route of FA-CPSP-UA are shown in Scheme 1. CPSP composed of spermine and CBA was successfully synthesized by Michael addition reaction. UA and FA were attached to the CPSP through amide bonds in a one-step reaction. As shown in Fig. 1, ^1H NMR analysis demonstrated

the CPSP and FA-CPSP-UA were synthesized successfully. According to the ^1H NMR spectra of FA and UA, the peaks at 0.5–1.0 ppm and 7.0–9.0 ppm were the characteristic peaks of UA and FA, respectively [43,44]. Moreover, the ^1H NMR spectrum of the FA-CPSP-UA in DMSO- d_6 was measured and the chemical structure of UA and FA are added in Fig. S1. UV-vis spectrum was used to confirm the presence and mass content of UA and FA conjugation on CPSP. As shown in Fig. 2, FA exhibited the obvious absorbance peaks at 378 nm and UA showed the obvious absorbance peaks at 270 nm, at which CPSP showed no peaks. The UA and FA mass content in FA-CPSP-UA were 20.13% and 17.3% using a standard calibration curve.

$$A_{\text{FA},1} = A_{378}$$

$$A_{\text{UA}} = A_{270} - A_{\text{FA},2}$$

Where A_{378} and A_{270} are the absorbance values of FA-CPSP-UA at 378 nm and 270 nm respectively.

$A_{\text{FA},1}$ and $A_{\text{FA},2}$ are the absorbance values of FA conjugation on CPSP at 378 nm and 270 nm respectively. A_{UA} is the absorbance values of UA conjugation on CPSP.

Zeta potential of the CPSP, UA-CPSP ($W_{\text{UA}} = 22.4\%$) and FA-CPSP-UA, which were diluted in deionized water solutions, was measured. As shown in Fig. 2A, the surface charge of CPSP was about +42.43 mV due to the amine groups on its surface, while the zeta potentials of UA-CPSP and FA-CPSP-UA were $+35.57 \pm 0.91$ mV and $+27.5 \pm 1.53$ mV, respectively. Prodrug with positive charges often exhibit the higher cellular uptakes than the neutral and negatively charged prodrug due to their electrostatic interactions with the anionic membrane [41,45–47]. In Fig. 2B, the particle size of the CPSP, UA-CPSP, FA-CPSP-UA, which were diluted with ultrapure water at 100 $\mu\text{g}/\text{mL}$, was determined by dynamic light scattering method. The particle sizes of CPSP, UA-CPSP ($W_{\text{UA}} = 22.4\%$) and FA-CPSP-UA were 404.7 ± 8.33 nm, 186.4 ± 5.20 nm and 223.3 ± 11.17 nm, respectively.

3.2. The GSH-responsive of FA-CPSP-UA

We used TEM analysis to study the effect of GSH on FA-CPSP-UA nanoparticle morphology. As shown in Fig. 3C and D, the particle size of FA-CPSP-UA obviously reduced after FA-CPSP-UA was treated with 10 mM GSH. This result suggested that FA-CPSP-UA could significant degrade at the concentration of 10 mM GSH. Disulfide bonds were known to be easily cleaved by GSH in the reducing conditions [48,49]. For further examining the GSH-Sensitive of FA-CPSP-UA, GPC analysis was performed and the chromatograms of FA-CPSP-UA treated with or without 10 mM GSH are shown in Fig. 3E. It was found that FA-CPSP-UA without GSH treatment showed the maximum peak at 7.44 min. After incubation with 10 mM GSH for 4 h, the maximum peak of the sample shifted to 8.09 min, which indicated that GSH resulted in the breakage of disulfide bonds and obvious degradation of FA-CPSP-UA. This result was consistent with TEM analysis, suggesting the potential application of FA-CPSP-UA as a redox-responsive delivery system to tumor cells.

The release properties of UA from FA-CPSP-UA were measured under 10 mM GSH, due to the intracellular concentration of GSH can reach 10 mM. As shown in Fig. 3F, the ratios of released UA in the different buffers all increased in a time dependent manner. In addition, UA release from FA-CPSP-UA was markedly enhanced under a reductive condition containing 10 mM GSH, wherein about 64% drug was released in 24 h. FA-CPSP-UA exhibited a rapid release in 10 mM GSH, which may be conducive to tumor therapy.

3.3. FA-targeting assay

To more directly define a role for FA targeting, the MCF-7 cells were selected to perform the cellular uptake studies. MCF-7 cells highly expressed FRs, and FRs are expressed at low levels in normal tissues [50].

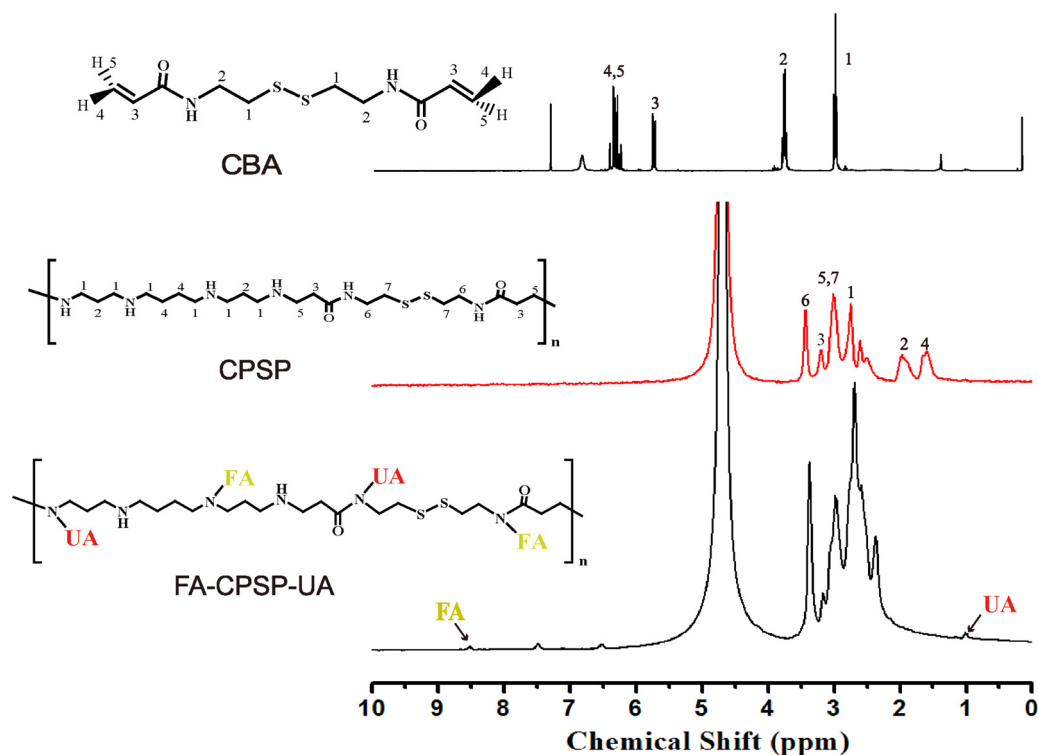


Fig. 1. Characterization of representative ^1H NMR spectra of N,N'-cystaminebisacrylamide (CBA), CPSP and FA-CPSP-UA.

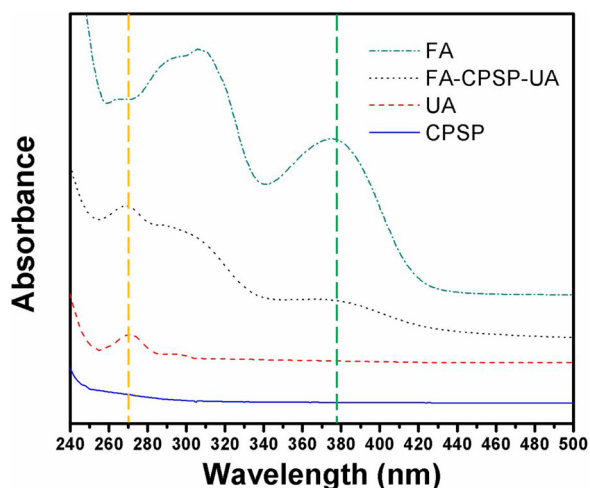


Fig. 2. UV-vis spectra of FA, UA, CPSP and FA-CPSP-UA (25 °C).

Receptor-mediated endocytosis of FA-CPSP-UA was defined by carrying out competitive experiments under the same experimental conditions. Seen in Fig. 4C, with the increase free FA concentration, the endocytosis of MCF-7 cells treated with FA-CPSP-UA obviously decreased, but they of MCF-7 cells treated with CPSP-UA are slightly affected. The FR-mediated endocytosis can be blocked by free FA. The above results demonstrated that the targeting ability of FA-CPSP-UA to high FRs expressed in MCF-7 cells. These results indicated that the FA-CPSP-UA could enter FR over-expressing cancer cells by the electrostatic interaction, and the ligand-receptor mediation.

3.4. In vitro cytotoxicity

MCF-7 cells were chosen to evaluate the anti-tumor effect of prodrugs, and the results were shown in Fig. 4E. For ensuring the comparison of the experiment, the corresponding concentrations of UA-

CPSP and FA-CPSP-UA were calculated according to the grafting rate of UA. The results shown that both the formulations showed a typical dose-dependent cytotoxic effect on MCF-7 cells. To our surprise, FA-CPSP-UA and UA-CPSP showed superior anticancer effect than free UA in the UA concentration range of 10–25 $\mu\text{g}/\text{mL}$. The results showed that FA-CPSP-UA and UA-CPSP not only maintained the pharmacological action of UA but also enhanced its anticancer effect by the chemosensitizing effects. Furthermore, FA-modified prodrugs showed finer MCF-7 cells inhibition efficiency than non-FA-modified ones (Fig. 4E). The superior cytotoxic effect of FA-CPSP-UA was attributed to the enhanced cellular uptake of the prodrugs *via* the FR mediated endocytosis.

Next, to evaluate the influence of intracellular GSH level on the UA efficacy, we investigated the cell inhibitory effects of UA in different intracellular GSH levels in MCF-7 cells. The cell viabilities are shown in Fig. 4F after different treatments for 24 h, Free BSO and Free GSH had a negligible reduction in cell viability. Nevertheless, the cytotoxicity of UA obviously increased to MCF-7 cells after co-treated with BSO, in which BSO displayed the similar effect with CPSP. The results proved that a down-regulated GSH expression does improve the sensibility of tumor cells to chemical chemotherapeutics, and the excellent tumor cells inhibition effect of FA-CPSP-UA was attributed to its chemosensitizing effect.

3.5. Effects of UA, FA-CPSP and FA-CPSP-UA on levels of intracellular GSH

It is universally acknowledged that GSH is a tripeptide evolved in many important cellular roles as a redox regulator. The concentration level of intracellular GSH in some tumor cells has been found to be several times higher than that in normal cells. Cancer cells are in permanent oxidative stress compensating by up-regulation of the GSH synthesis pathway. A decrease in the intracellular GSH level by an effective GSH-depleting compound can inhibit GSH-mediated detoxification. In order to determine influence of FA-CPSP-UA on intracellular GSH, we detected intracellular GSH concentration in MCF-7 cells after treated with different samples. As shown in Fig. 4D,

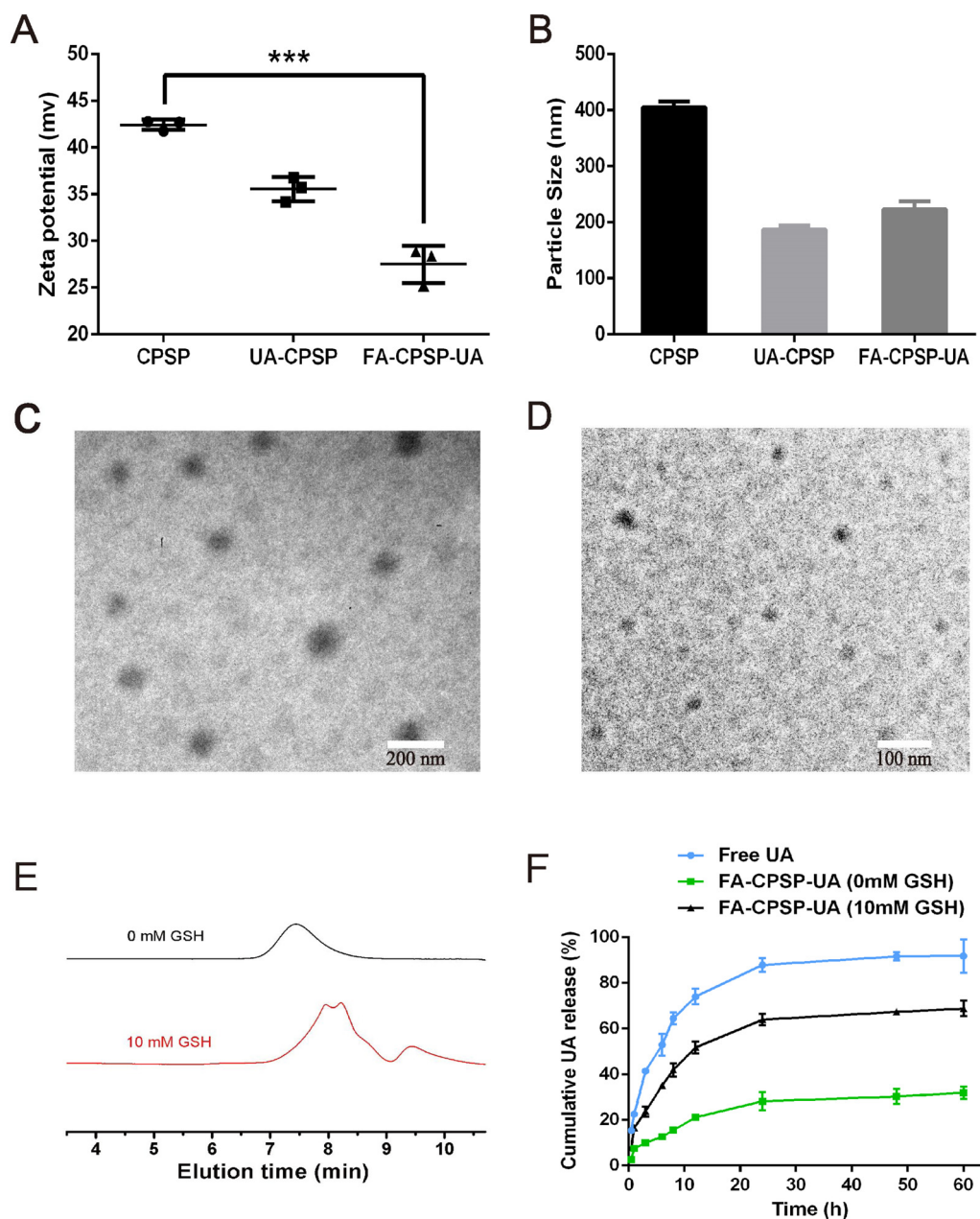


Fig. 3. (A) Zeta potential analysis of CPSP, UA-CPSP and FA-CPSP-UA; (B) Particle size of CPSP, UA-CPSP and FA-CPSP-UA; (C) TEM photographs of FA-CPSP-UA (scale bar: 200 nm); (D) TEM photographs of FA-CPSP-UA treated with 10 mM GSH (scale bar: 100 nm); (E) GPC chromatogram of FA-CPSP-UA pretreated either with or without 10 mM GSH. (using dextran as the standard sample; 0.8 mol/L NaNO₃; 35 °C); (F) *in vitro* release of UA. The percentages of released UA are compared between free UA and FA-CPSP-UA in PBS (with or without 10 mM GSH) at pH 7.4 and 37 °C.

compared to treatments with UA, treatments with other four samples significantly reduced the concentration of intracellular GSH. L-buthionine-S,R-sulfoximine (BSO) is an inhibitor of GSH biosynthesis. As expected, after the treatments of BSO contained agents, GSH in MCF-7 cells apparently decreases. Moreover, compared to the treatments by BSO, FA-CPSP leads to an almost same GSH depleting effect. The result confirmed that FA-CPSP and FA-CPSP-UA showed the similar ability of down-regulating GSH expression with BSO in the MCF-7 cells, further affirming that the chemosensitizing effects of FA-CPSP-UA was induced by the depletion of intracellular GSH.

3.6. Apoptosis effect

Many studies have demonstrated that tumors are closely related to cellular apoptosis. When cellular apoptosis is inhibited, tumors occur

and grow. Thus, through cell apoptosis assay to further determine the superior anticancer effect of prodrugs. Annexin V/PI double staining characterized the apoptosis effect. The difference in translocation of phosphatidyl serine (PS) from outer surface in normal cells to the outer leaflet of the cell membrane in apoptotic cells aids the evaluation of cell apoptosis. Annexin-V, could bind with PS with a high affinity and identify apoptotic cells by binding to PS exposed on the outer leaflet. Additionally, dead cells could be stained with propidium iodide (PI) dye. Thus, after staining a cell population with annexin V-FITC and PI, apoptotic cells exhibit green fluorescence, dead cells exhibit red fluorescence, and live cells exhibit little or no fluorescence [51]. As showed in Fig. 5A and B, the cells treated with PBS and CPSP did not show any noticeable apoptosis, which further illustrated CPSP non-cytotoxicity. After treated with free UA, UA-CPSP and FA-CPSP-UA for 24 h, MCF-7 cells exhibited 28.62%, 38.76% and 50.78% apoptosis, respectively.

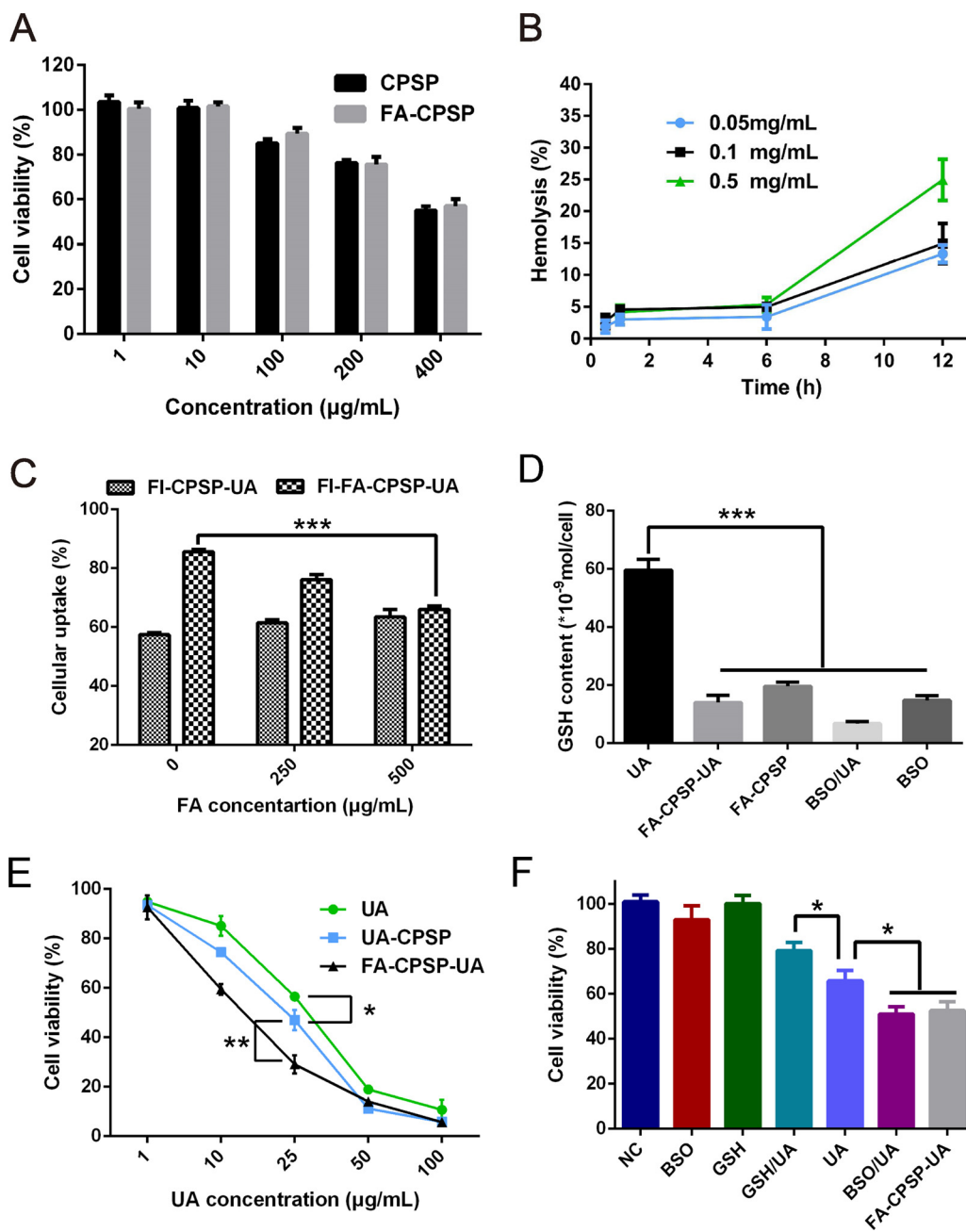


Fig. 4. (A) Survival rate analysis of MCF-7 cells after treating with CPSP and FA-CPSP at different concentrations; (B) Effect of FA-CPSP-UA with different concentrations on hemolysis; (C) Cellular uptake ratios of materials after being incubated with normal or FA-pretreated MCF-7 cells; (D) Intracellular GSH concentration in MCF-7 cells after MCF-7 cells were incubated with free UA, FA-CPSP-UA, FA-CPSP, BSO/UA and BSO; (E) The survival rates of MCF-7 are compared between free UA, UA-CPSP and FA-CPSP-UA at different concentrations; (F) MCF-7 cells were incubated with BSO, GSH, GSH/UA, free UA, BSO/UA and FA-CPSP-UA. PBS was set as the control and the survival rate was evaluated by CCK-8 assay.

UA, UA-CPSP and FA-CPSP-UA could significantly cause the early and late apoptosis in MCF-7 cells, in comparison to the free drug, the pro-drugs can be more effective on cell apoptosis under the same drug concentration.

3.7. Inhibited migration of MCF-7 cells and metastasis related protein expression

It was reported that over 90% of the deaths of cancer patients is caused by metastasis, which is formed by the spread of disseminated primary tumor cells to distant anatomic sites [52]. Matrix metalloproteinase-9 (MMP-9) was vital in the progression of tumor metastasis [53]. Hence, the down-regulation of the expression of MMP-9 protein would be a good way to inhibited migration of tumor cells. The cellular expression levels of MMP-9 protein in FA-CPSP-UA-treated MCF-7 cells were examined by Western blotting analysis. Fig. 7A shows the image of gel electrophoresis, and the relative quantitative MMP-9 protein

expression result is shown in Fig. 7B. It was found that, compared to the control, FA-CPSP-UA effectively inhibited the expression of MMP-9 in MCF-7 cells in a dose-dependent manner.

To further validate the inhibited migration effect of FA-CPSP-UA, a wound healing assay is conducted to analyze the impact of the low toxicity concentrations of FA-CPSP-UA on migration of MCF-7 cells (Fig. 6C). As shown in Fig. 6, compared with the control, the migration of MCF-7 cells were remarkably inhibited by FA-CPSP-UA in a dose-dependent manner (the quantitative data are given in Fig. 6B). This result suggested that FA-CPSP-UA efficiently inhibited migration of MCF-7 cells by inhibiting MMP-9 protein expression.

3.8. Hemolysis and toxicity

The cytotoxicity of CPSP and FA-CPSP was evaluated on MCF-7 cells by CCK-8 assay in Fig. 4A. It shows the cell viability results of the MCF-7 cells treated with different concentrations for 24 h. As shown, CPSP

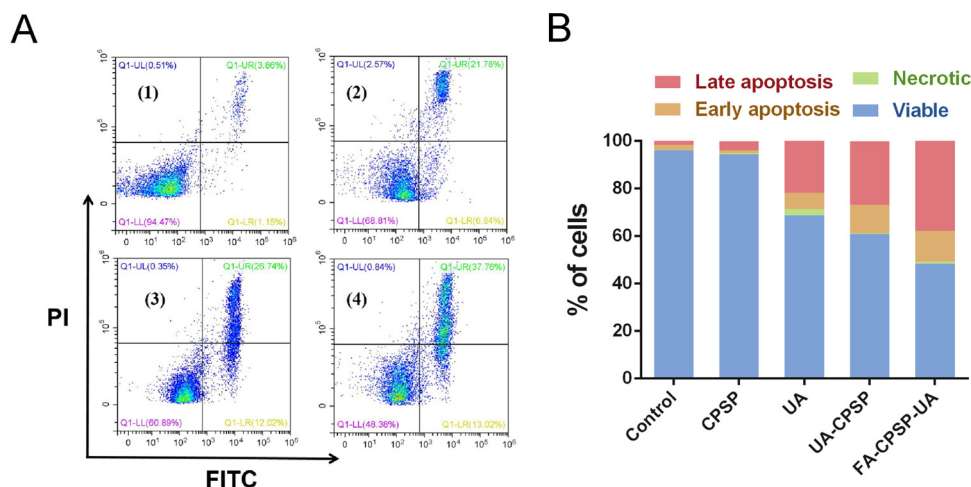


Fig. 5. Apoptosis analysis (A and B) of MCF-7 cells evaluated by flow cytometer after MCF-7 cells were incubated with various samples. (1) CPSP; (2) UA; (3) UA-CPSP; (4) FA-CPSP-UA; (5) PBS was set as the control.

and FA-CPSP showed almost the same cytotoxicity to MCF-7 cells, and the cell survival rate is 74.1% when the concentration reached 200 $\mu\text{g}/\text{mL}$. This result indicated that CPSP was evaluated to confirm its safety. To evaluate the blood compatibility of prodrug, hemolysis test was carried out. As an injectable drug delivery system, the instability of drug carriers in the blood was considered as one of the serious

limitations in the therapeutic. The percentages hemolysis of the blood in contact with FA-CPSP-UA concentration are shown in Fig. 4B. After 6 h incubation, all the sample showed nonhemolytic with the extent of hemolysis lower than the permissible level of 5%. It was found that FA-CPSP-UA exhibited the good blood compatibility at the low concentration.

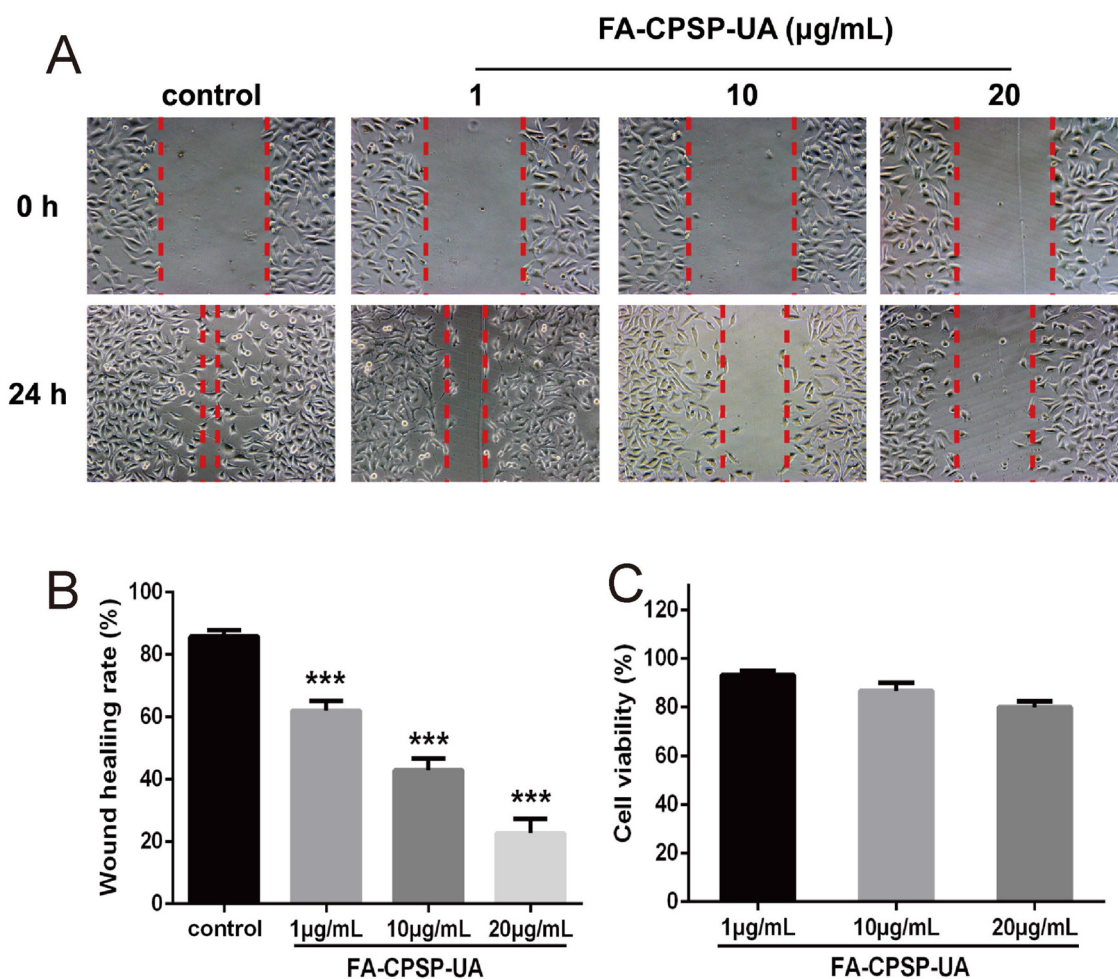


Fig. 6. The effect of FA-CPSP-UA on the migratory abilities of MCF-7 cells. (A) FA-CPSP-UA inhibited the migration of MCF-7 cells; (B) the effect of FA-CPSP-UA on the relative number of migrating cells; (C) the low toxicity of FA-CPSP-UA to MCF-7 cells at the same concentration as used in the migration assay.

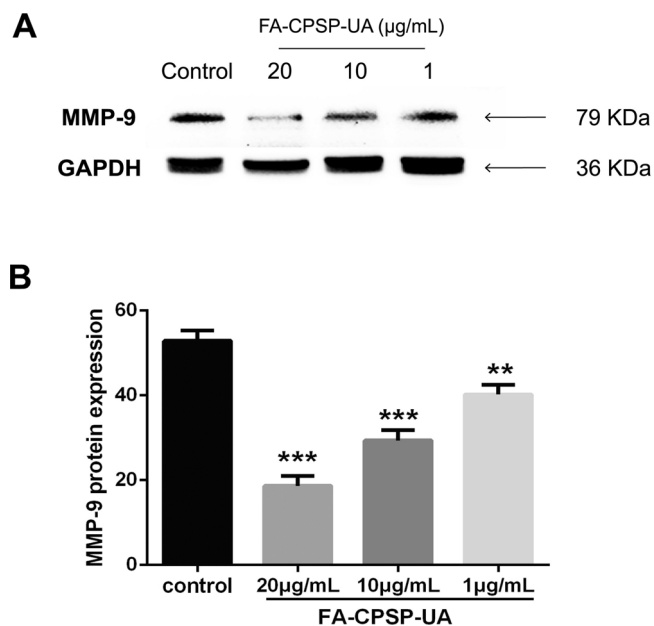


Fig. 7. (A) Representative MMP-9 protein expression determined by Western blot analysis; (B) Analysis of light intensities of MMP-9 protein expression as the ratio of MMP-9 to GAPDH from Western blot results.

4. Conclusions

In the present investigation, a targeted chemosensitive anticancer prodrug (FA-CPSP-UA) has been successfully synthesized and used to treat human breast tumor. The CPSP modified with UA and FA targeting moieties showed high aqueous solubility, GSH-triggered degradation and good biocompatibility. The FA-CPSP-UA exhibited excellent selectivity towards tumor cells, through utilizing the main pathways of absorption endocytosis and receptor-mediated endocytosis. Moreover, FA-CPSP-UA could down-regulate the generation of GSH and manifest excellent ability in enhancing antitumor efficacy. In addition, FA-CPSP-UA could inhibit the expression of MMP-9, which led to inhibit MCF-7 cells migration. Taken together, the results indicated that FA-CPSP-UA, as a carrier, can efficiently deliver UA to folate receptor positive cancer cells and improve tumor therapy of UA by Chemosensitive effect.

Acknowledgment

This work was financially supported by the fund from Guangzhou Science and Technology Program (201607010127).

Appendix A. Supplementary data

Supplementary material related to this article can be found, in the online version, at doi:<https://doi.org/10.1016/j.colsurfb.2018.06.029>.

References

- L. Xiang, T. Chi, Q. Tang, X. Yang, M. Ou, X. Chen, et al., A pentacyclic triterpene natural product, ursolic acid and its prodrug US597 inhibit targets within cell adhesion pathway and prevent cancer metastasis, *Oncotarget* 6 (2015) 9295–9312.
- D. Kashyap, H.S. Tuli, A.K. Sharma, Ursolic acid (UA): a metabolite with promising therapeutic potential, *Life Sci.* 146 (2016) 201–213.
- S. Prasad, V.R. Yadav, R. Kannappan, B.B. Aggarwal, Ursolic acid, a pentacyclic triterpene, potentiates TRAIL-induced apoptosis through p53-independent up-regulation of death receptors evidence for the role of reactive oxygen species and JNK (retracted article. See vol. 291, pg. 16924, 2016), *J. Biol. Chem.* 286 (2011) 5546–5557.
- J.-Q. Ma, J. Ding, Z.-H. Xiao, C.-M. Liu, Ursolic acid ameliorates mouse tetra-chloride-induced oxidative DNA damage and inflammation in carbon kidney by inhibiting the STAT3 and NF-kappa B activities, *Int. Immunopharmacol.* 21 (2014) 389–395.
- R. Saravanan, P. Viswanathan, K.V. Pugalendi, Protective effect of ursolic acid on ethanol-mediated experimental liver damage in rats, *Life Sci.* 78 (2006) 713–718.
- M.-Y. Qi, J.-J. Yang, B. Zhou, D.-Y. Pan, X. Sun, Study on the protective effect of ursolic acid on alloxan-induced diabetic renal injury and its underlying mechanisms, *Chin. J. Appl. Physiol.* 30 (2014) 445–448.
- J.-s. Wang, T.-n. Ren, T. Xi, Ursolic acid induces apoptosis by suppressing the expression of FoxM1 in MCF-7 human breast cancer cells, *Med. Oncol.* 29 (2012) 10–15.
- S. Saraswati, S.S. Agrawal, A.A. Alhaider, Ursolic acid inhibits tumor angiogenesis and induces apoptosis through mitochondrial-dependent pathway in Ehrlich ascites carcinoma tumor, *Chem. Biol. Interact.* 206 (2013) 153–165.
- A. Jedinak, M. Muckova, D. Kost'alo, T. Maliar, I. Materova, Antiprotease and antimetastatic activity of ursolic acid isolated from *Salvia officinalis*, *Zeitschrift Fur Naturforschung C-J. Biosci.* 61 (2006) 777–782.
- W. Gu, X.-Y. Jin, D.-D. Li, S.-F. Wang, X.-B. Tao, H. Chen, Design, synthesis and in vitro anticancer activity of novel quinoline and oxadiazole derivatives of ursolic acid, *Bioorg. Med. Chem. Lett.* 27 (2017) 4128–4132.
- E. Kassi, T.G. Sourlingas, M. Spiliotaki, Z. Papoutsis, H. Pratsinis, N. Aliogiannis, et al., Ursolic acid triggers apoptosis and Bcl-2 downregulation in MCF-7, *Breast Cancer Cells Cancer Investig.* 27 (2009) 723–733.
- H. Zhang, X. Li, J. Ding, H. Xu, X. Dai, Z. Hou, et al., Delivery of ursolic acid (UA) in polymeric nanoparticles effectively promotes the apoptosis of gastric cancer cells through enhanced inhibition of cyclooxygenase 2 (COX-2), *Int. J. Pharm.* 441 (2013) 261–268.
- X.J. Zhou, X.M. Hu, Y.M. Yi, J. Wan, Preparation and body distribution of freeze-dried powder of ursolic acid phospholipid nanoparticles, *Drug Dev. Ind. Pharm.* 35 (2009) 305–310.
- G. Yang, T. Yang, W. Zhang, M. Lu, X. Ma, G. Xiang, In vitro and in vivo antitumor effects of folate-targeted ursolic acid stealth liposome, *J. Agric. Food Chem.* 62 (2014) 2207–2215.
- H. Zhang, D. Zheng, J. Ding, H. Xu, X. Li, W. Sun, Efficient delivery of ursolic acid by poly(N-vinylpyrrolidone)-block-poly (epsilon-caprolactone) nanoparticles for inhibiting the growth of hepatocellular carcinoma, *Int. J. Nanomed.* 10 (2015) 1909–1920.
- Y. Gao, Z. Li, X. Xie, C. Wang, J. You, F. Mo, et al., Dendrimeric anticancer prodrugs for targeted delivery of ursolic acid to folate receptor-expressing cancer cells: synthesis and biological evaluation, *Eur. J. Pharm. Sci.* 70 (2015) 55–63.
- D. Peer, J.M. Karp, S. Hong, O.C. Farokhzad, R. Margalit, R. Langer, Nanocarriers as an emerging platform for cancer therapy, *Nat. Nanotechnol.* 2 (2007) 751–760.
- B. Wang, Y.-F. Xu, B.-S. He, Y.-Q. Pan, L.-R. Zhang, C. Zhu, et al., RNAi-mediated silencing of CD147 inhibits tumor cell proliferation, invasion and increases chemosensitivity to cisplatin in SGC7901 cells in vitro, *J. Exp. Clin. Cancer Res.* 29 (2010).
- G.-Y. Chen, C.-L. Meng, K.-C. Lin, H.-Y. Tuan, H.-J. Yang, C.-L. Chen, et al., Graphene oxide as a chemosensitizer: diverted autophagic flux, enhanced nuclear import, elevated necrosis and improved antitumor effects, *Biomaterials* 40 (2015) 12–22.
- E. Gullotti, Y. Yeo, Extracellularly activated nanocarriers: a new paradigm of tumor targeted drug delivery, *Mol. Pharm.* 6 (2009) 1041–1051.
- S.D. Weitman, R.H. Lark, L.R. Coney, D.W. Fort, V. Frasca, V.R. Zurawski Jr. et al., Distribution of the folate receptor GP38 in normal and malignant cell lines and tissues, *Cancer Res.* 52 (1992) 3396–3401.
- J.F. Ross, P.K. Chaudhuri, M. Ratnam, Differential regulation of folate receptor isoforms in normal and malignant tissues and in established cell lines. Physiologic and clinical implications, *Cancer* 73 (1994) 2432–2443.
- A.C. Antony, M.A. Kane, R.M. Portillo, P.C. Elwood, J.F. Kolhouse, Studies of the role of a particulate folate-binding protein in the uptake of 5-methyltetrahydrofolate by cultured human KB cells, *J. Biol. Chem.* 260 (1985) 14911–14917.
- S. Xiao, C. Tong, X. Liu, D. Yu, Q. Liu, C. Xue, et al., Preparation of folate-conjugated starch nanoparticles and its application to tumor-targeted drug delivery vector, *Chin. Sci. Bull.* 51 (2006) 1693–1697.
- G. Szakacs, M.D. Hall, M.M. Gottesman, A. Boumendjel, R. Kachadourian, B.J. Day, et al., Targeting the Achilles heel of multidrug-resistant cancer by exploiting the fitness cost of resistance, *Chem. Rev.* 114 (2014) 5753–5774.
- X. Zhang, F.-G. Wu, P. Liu, N. Gu, Z. Chen, Enhanced fluorescence of gold nanoclusters composed of H₂AuCl₄ and histidine by glutathione: glutathione detection and selective cancer cell imaging, *Small* 10 (2014) 5170–5177.
- J.M. Estrela, A. Ortega, E. Obrador, Glutathione in cancer biology and therapy, *Crit. Rev. Clin. Lab. Sci.* 43 (2006) 143–181.
- F. Lopes-Coelho, S. Gouveia-Fernandes, L.G. Goncalves, C. Nunes, I. Faustino, F. Silva, et al., HNF1 beta drives glutathione (GSH) synthesis underlying intrinsic carboplatin resistance of ovarian clear cell carcinoma (OCCC), *Tumor Biol.* 37 (2016) 4813–4829.
- M.-Q. Gong, C. Wu, X.-Y. He, J.-Y. Zong, J.-L. Wu, R.-X. Zhuo, et al., Tumor targeting synergistic drug delivery by self-assembled hybrid nanovesicles to overcome drug resistance, *Pharm. Res.* 34 (2017) 148–160.
- A. Cunningham, J.K. Oh, New design of thiol-responsive degradable poly(lactide)-based block copolymer micelles, *Macromol. Rapid Commun.* 34 (2013) 163–168.
- N.R. Ko, J.K. Oh, Glutathione-triggered disassembly of dual disulfide located degradable nanocarriers of poly(lactide)-based block copolymers for rapid drug release, *Biomacromolecules* 15 (2014) 3180–3189.
- X. Zhao, P. Liu, Reduction-responsive core-shell-corona micelles based on triblock copolymers: novel synthetic strategy, characterization, and application as a tumor microenvironment-responsive drug delivery system, *ACS Appl. Mater. Interfaces* 7 (2015) 166–174.

- [33] Q. Zhang, J. He, M. Zhang, P. Ni, A polyphosphoester-conjugated camptothecin prodrug with disulfide linkage for potent reduction-triggered drug delivery, *J. Mater. Chem. B* 3 (2015) 4922–4932.
- [34] Z.B. Li, X.J. Loh, Water soluble polyhydroxyalkanoates: future materials for therapeutic applications, *Chem. Soc. Rev.* 44 (2015) 2865–2879.
- [35] D. Ma, X.-Y. Zhou, Y.-F. Yang, Y. You, Z.-H. Liu, J.-T. Lin, et al., UV cross-linked redox-responsive hydrogels for co-delivery of hydrophilic and hydrophobic drugs, *Sci. Adv. Mater.* 5 (2013) 1307–1315.
- [36] Y. Gu, Y. Guo, C. Wang, J. Xu, J. Wu, T.B. Kirk, et al., A polyamidoamine dendrimer functionalized graphene oxide for DOX and MMP-9 shRNA plasmid co-delivery, *Mater. Sci. Eng. C-Mater. Biol. Appl.* 70 (2017) 572–585.
- [37] D. Ma, Q.-M. Lin, L.-M. Zhang, Y.-Y. Liang, W. Xue, A star-shaped porphyrin-arginine functionalized poly(L-lysine) copolymer for photo-enhanced drug and gene co-delivery, *Biomaterials* 35 (2014) 4357–4367.
- [38] G. Jiao, X. He, X. Li, J. Qiu, H. Xu, N. Zhang, et al., Limitations of MTT and CCK-8 assay for evaluation of graphene cytotoxicity, *RSC Adv.* 5 (2015) 53240–53244.
- [39] I. Vermes, C. Haanen, H. Steffens-Nakken, C. Reutelingsperger, A novel assay for apoptosis. Flow cytometric detection of phosphatidylserine expression on early apoptotic cells using fluorescein labelled Annexin V, *J. Immunol. Methods* 184 (1995) 39–51.
- [40] H. Hu, Y. You, L. He, T. Chen, The rational design of NAMI-A-loaded mesoporous silica nanoparticles as antiangiogenic nanosystems, *J. Mater. Chem. B* 3 (2015) 6338–6346.
- [41] P. Xu, H. Yu, Z. Zhang, Q. Meng, H. Sun, X. Chen, et al., Hydrogen-bonded and reduction-responsive micelles loading atorvastatin for therapy of breast cancer metastasis, *Biomaterials* 35 (2014) 7574–7587.
- [42] Y. Zhang, J. Cai, C. Li, J. Wei, Z. Liu, W. Xue, Effects of thermosensitive poly-(N-isopropylacrylamide) on blood coagulation, *J. Mater. Chem. B* 4 (2016) 3733–3749.
- [43] Y. Kashiwada, T. Nagao, A. Hashimoto, Y. Ikeshiro, H. Okabe, L.M. Cosentino, et al., Anti-AIDS agents 38. Anti-HIV activity of 3-O-acyl ursolic acid derivatives, *J. Nat. Prod.* 63 (2000) 1619–1622.
- [44] Y. Zhang, T.P. Thomas, A. Desai, H. Zong, P.R. Leroueil, I.J. Majoros, et al., Targeted dendrimeric anticancer prodrug: a methotrexate-folic acid-poly(amidoamine) conjugate and a novel, rapid, “one pot” synthetic approach, *Bioconj. Chem.* 21 (2010) 489–495.
- [45] X. Zeng, W. Tao, L. Mei, L. Huang, C. Tan, S.-S. Feng, Cholic acid-functionalized nanoparticles of star-shaped PLGA-vitamin E TPGS copolymer for docetaxel delivery to cervical cancer, *Biomaterials* 34 (2013) 6058–6067.
- [46] M. Huang, K. Zhao, L. Wang, S. Lin, J. Li, J. Chen, et al., Dual stimuli-responsive polymer prodrugs quantitatively loaded by nanoparticles for enhanced cellular internalization and triggered drug release, *ACS Appl. Mater. Interfaces* 8 (2016) 11226–11236.
- [47] X. Guo, X. Wei, Y. Jing, S. Zhou, Size changeable nanocarriers with nuclear targeting for effectively overcoming multidrug resistance in cancer therapy, *Adv. Mater.* 27 (2015) 6450.
- [48] M.H. Lee, Z. Yang, C.W. Lim, Y.H. Lee, S. Dongbang, C. Kang, et al., Disulfide-cleavage-triggered chemosensors and their biological applications, *Chem. Rev.* 113 (2013) 5071–5109.
- [49] Y. Su, Y. Hu, Y. Du, X. Huang, J. He, J. You, et al., Redox-responsive polymer drug conjugates based on doxorubicin and chitosan oligosaccharide-g-stearic acid for cancer therapy, *Mol. Pharm.* 12 (2015) 1193–1202.
- [50] L. Sun, Z. Wei, H. Chen, J. Liu, J. Guo, M. Cao, et al., Folic acid-functionalized up-conversion nanoparticles: toxicity studies and targeted imaging applications, *Nanoscale* 6 (2014) 8878–8883.
- [51] M. Luo, X. Liu, Y. Zu, Y. Fu, S. Zhang, L. Yao, et al., Cajanol, a novel anticancer agent from *Pigeonpea* *Cajanus cajan* (L.) Millsp. roots, induces apoptosis in human breast cancer cells through a ROS-mediated mitochondrial pathway, *Chem. Biol. Interact.* 188 (2010) 151–160.
- [52] J.-X. Fan, D.-W. Zheng, L. Rong, J.-Y. Zhu, S. Hong, C. Li, et al., Targeting epithelial-mesenchymal transition: metal organic network nano-complexes for preventing tumor metastasis, *Biomaterials* 139 (2017) 116–126.
- [53] M. Steinhagen, P.-G. Hoffmeister, K. Nordsieck, R. Hoetzel, L. Baumann, M.C. Hacker, et al., Matrix metalloproteinase 9 (MMP-9) mediated release of MMP-9 resistant stromal cell-derived factor 1 alpha (SDF-1 alpha) from surface modified polymer films, *ACS Appl. Mater. Interfaces* 6 (2014) 5891–5899.